Int. J. Electrochem. Sci., 11 **(2016)** 9566 – 9574, doi: 10.20964/2016.11.72

International Journal of
ELECTROCHEMICAL
SCIENCE
www.electrochemsci.org

Short Communication

Graphene-Supported Silver Nanoparticles with High Activities toward Chemical Catalytic Reduction of Methylene Blue and Electrocatalytic Oxidation of Hydrazine

Chengen He[1], *Zixiu Liu*[1], *Yun Lu*[1], *Leping Huang*[2,*], *and Yingkui Yang* [1,*]

[1] School of Materials Science and Engineering, Hubei University, Wuhan 430062, China
[2] School of Materials Science and Engineering, Wuhan Textile University, Wuhan 430200, China
[*]E-mail: lphuang@wtu.edu.cn, ykyang@hubu.edu.cn

Received: 27 June 2016 / *Accepted:* 7 September 2016 / *Published:* 10 October 2016

Reduced graphene oxide (RGO)/silver nanoparticle (Ag NP) composites (Ag/RGO) were prepared by a two-step route that involves chelating Ag NPs onto GO in the presence of *N*, *N*-dimethylformamide, followed by reduction with sodium borohydride. Ag NPs with an average dimeter of 5.6 nm were found to be uniformly distributed on the surface of RGO sheets, and the resulting Ag/RGO composite exhibits good chemical catalytic behavior toward reduction of methylene blue and high electrocatalytic activity toward electrooxidation of hydrazine.

Keywords: Reduced graphene oxide, silver nanoparticles, chemical catalysis, electrocatalysis.

1. INTRODUCTION

High specific surface area and excellent electrical transportation are some of the outstanding properties that make graphene an ideal template for fabricating graphene-metal nanocomposites. Graphene-metal nanocomposites combine the attractive properties of graphene with those of metal nanoparticles (MNPs) and have been applied in a wide variety of fields such as electrochemical sensing [1, 2], energy storage [3, 4], and catalysis [5, 6]. There are several different ways to produce graphene-metal nanocomposites, and the most straightforward approach is the chemical reduction of metal ions in the presence of graphene. However, graphene nanosheets tend to re-aggregate and even restack into the graphite form [7] if they are not decorated by stabilizers such as polymers [8, 9] or small molecules [10, 11]. Therefore, it would be very difficult for MNPs to intercalate and attach onto the surface of pure graphene nanosheets, resulting in a low metal-loading rate. On the contrary, hydrophilic graphene oxide (GO) can be exfoliated into isolated nanosheets to form stable suspensions

in some polar organic solvents [12], and the oxygenated groups of GO acting as nucleation sites that cause dense growth of MNPs [13]. The acquired nanocomposites have extensive potential applications such as effective surface-enhanced Raman scattering (SERS) substrates [14]. However, these oxygenated groups are chemically and/or thermally unstable. Huang [15] reported that the solution of Au nanoparticles/GO composite in *o*-nitroaniline converted to a black insoluble suspension after the catalytic reduction of *o*-nitroaniline by sodium borohydride ($NaBH_4$).

More importantly, GO sheets are electrically insulating, therefore, there is a need to restore the conjugated network of graphene. Reduced graphene oxide (RGO) can be achieved by removing oxygenated groups of GO through chemical or thermal treatments.[16, 17] As RGO has a much better electric conductivity and chemical stability, it became widely used especially in energy storage and electronic applications.[18] It is also noteworthy that some residual oxygenated groups in RGO due to the incomplete reduction can still maintain strong interaction with metal particles. It is reported that the silver-embedded GO nanocomposite (Ag/GO) was reduced by hydrazine vapors to produce silver-coated RGO nanocomposites (Ag/RGO), resulting in a 10^6-fold increase in electrical conductance [19].

In our previous work, silver nanoparticles (Ag NPs) were uniformly distributed on the surface of GO by using *N*, *N*-dimethylformamide (DMF) as a reductant of silver ions [20]. The as-fabricated Ag/GO composite was confirmed to be an excellent SERS-active substrate for molecule detecting. Herein the Ag/GO was further reduced by $NaBH_4$ to achieve the Ag/RGO composite, and its chemical catalysis and electrocatalytic properties were then studied.

2. EXPERIMENTAL

2.1. Materials

$NaBH_4$, methylene blue (MB), potassium sulfate (K_2SO_4), and hydrazine hydrate ($N_2H_4 \cdot H_2O$) were purchased from Sinopharm Chemical Reagent Co. Ltd (China) and were used as received.

2.2. Preparation of Ag/RGO nanocomposites

Typically, 8 mg of $AgNO_3$ was dispersed in 9 mL deionized water and then dropped into a previously prepared GO suspension (30 mg in 11 mL deionized water), which was sonicated for 30 min to form a stable colloid suspension. After that 20 mL of DMF was added under magnetic stirring and kept at 60°C for 6 h. Finally, the Ag/GO composite was obtained by filtrating and washing for several times with de-ionized water, and then vacuum drying at 60 °C. The Ag/RGO nanocomposites were produced by reducing the Ag/GO composites with $NaBH_4$ as the reductant. An appropriate amount of $NaBH_4$ was added into the Ag/GO suspension (in a mixed solvent of DMF and water, 4:1 in volume) and reacted at 80°C for 6 h under continuous stirring. As a strong reducing reagent, $NaBH_4$ functions effectively to reduce the oxygenated groups of GO, and thus transforming GO into RGO during the reaction process. Finally, the Ag/RGO nanocomposite was collected by filtration, and washed with de-ionized water to remove free Ag NPs, and finally vacuum-dried prior to measurements.

2.3. Characterization

Thermal gravimetric analysis (TGA) was carried out in a TGA-7 Perkin Elmer calorimeter at a heating rate of 20°C/min under argon flow (20 mL/min). X-ray diffraction (XRD) was conducted using a D/MAX-IIIC X-ray diffractometer with Cu Kα radiation. Transmission electron microscopy (TEM) and energy-dispersive spectroscopy (EDS) analysis were performed on a Tecnai G220 electron microscope at 200 kV. The particle size distribution of Ag NPs on RGO was measured using the software of Nano Measurer 1.2 with n >100 based on the TEM images.

We tested the chemical catalytic behaviors of Ag/RGO with respect to the reduction of MB by $NaBH_4$. First, 0.5 mL of the Ag/RGO suspension (0.5 mg/mL) was added to 80 mL of freshly prepared solution containing 4 mg MB and 8 mg $NaBH_4$, and the catalytic performance was then investigated with a UV-*vis* spectrometer to monitor the diversification of the dye absorbency.

Cyclic voltammetry (CV) scans were recorded with a conventional three-electrode system to study electrocatalytic characteristics of the Ag/RGO composite using an electrochemical workstation (BAS100B, USA), in which a platinum sheet and a saturated calomel electrode (SCE) were used as the counter electrode and the reference electrode, respectively. A glassy carbon electrode (GCE) (3 mm in diameter) was polished successively with 0.3 and 0.05 μm alumina powder, washed and sonicated with deionized water after each polishing step, and then dried under an infrared lamp before using it as the working electrode. Next, 10 μL of Ag/RGO suspension was dropped onto the surface of GCE and dried naturally at room temperature. The electrolyte (10 mM hydrazine in 0.1 M K_2SO_4 aqueous solution) was purged with N_2 for more than 30 min prior to measurements.

3. RESULTS AND DISCUSSION

3.1. Characterization of Ag/RGO composites

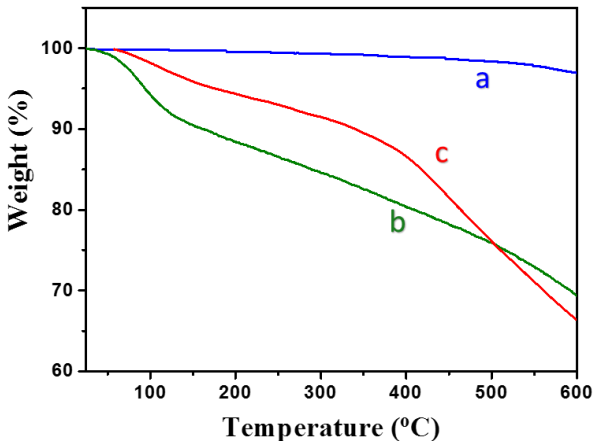

Figure 1. TGA curves of pristine graphite (a), RGO (b), and Ag/RGO (c).

Pristine graphite shows a trace of mass loss (3.2%) up to 600°C (Fig. 1a), while the overall weight loss of RGO is ~30% (Fig. 1b) owing to the dissociation of the residual oxygen-functional groups that were incompletely reduced by $NaBH_4$. The Ag/RGO (Fig. 1c) displays a similar profile but

less weight loss from 100 to 400°C, and the roughly constant difference in mass loss between RGO and Ag/RGO in this temperature range is ~7%, which is attributed to the absorbed Ag NPs around RGO. The drastic weight loss of Ag/RGO occurring after 400°C is attributed to the decomposition of residual oxygenated groups and C=C skeleton [21].

The crystalline structural changes were identified by XRD measurements. Pristine graphite shows a sharp peak (002) at 26.6° (Fig. 2a). The diffraction peak of RGO (Fig. 2b) became much broader with a small shifting to 23.4°, indicating that RGO has a less disordered structure and wider *d*-spacing (from 0.34 nm to 0.38 nm), which is due to the presence of residual oxygenated groups between RGO sheets [22].

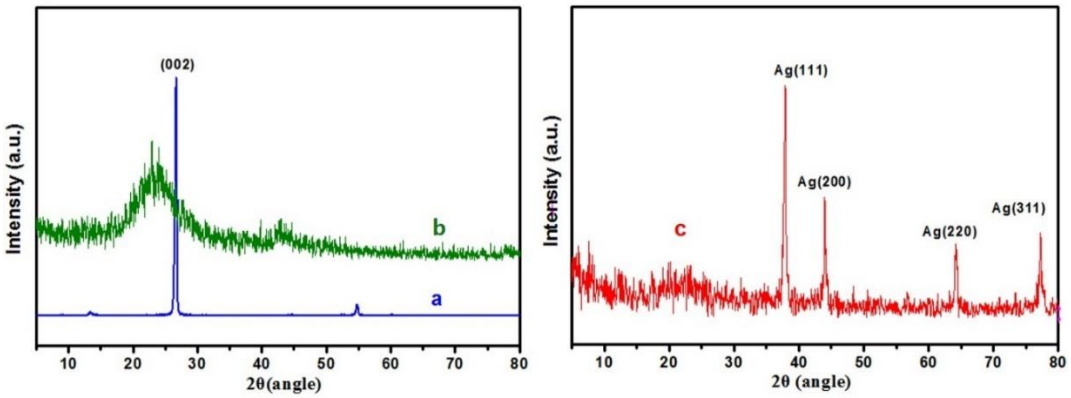

Figure 2. XRD spectra of pristine graphite (a), RGO (b), and Ag/RGO (c).

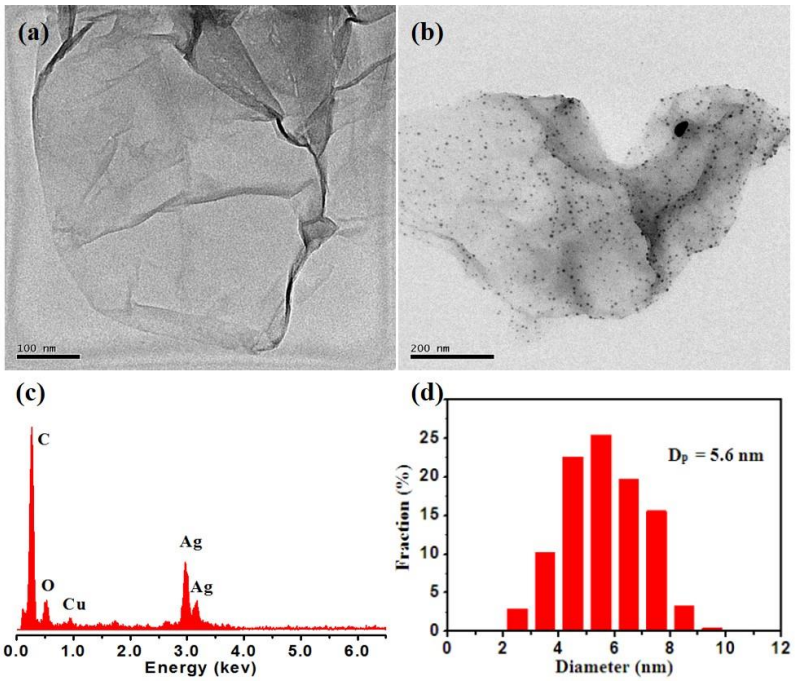

Figure 3. TEM images of (a) RGO, and (b) Ag/RGO; (c) EDX spectrum; and (d) Ag NP particle size distribution data of Ag/RGO (particle number fraction versus particle diameter).

The XRD spectrogram of the Ag/RGO composite (Fig. 2c) shows four characteristic diffraction peaks appearing at 2θ = 38.5°, 44.8°, 64.7°, and 77.8°, which can be assigned to the (111), (200), (220), and (311) crystalline planes of Ag, respectively [14]; however, no substantial diffraction peaks of RGO were observed, confirming that Ag NPs prevented the surface-to-surface stacks of RGO nanosheets [23, 24].

The TEM image of RGO (Fig. 3a) shows some scrolling on the edge of the thin layer and no obvious signs of impurities. In comparison, the images of Ag/RGO (Fig. 3b) clearly show that individual Ag NPs are present uniformly on the surface of RGO. The average size (D_p) of Ag NPs is estimated to be 5.6 nm with a narrow distribution (Fig. 3d), sharing the same morphological structure to Ag/GO as we reported previously [20]. Such morphological structure would provide a larger reaction interface and improve the catalytic activity. The EDS spectrum (Fig. 3c) clearly identifies the existence of atomic silver, oxygen, and carbon in the composite.

3.2. Chemical catalytic property of Ag/RGO

It is known that noble MNPs with small size and narrow size distribution usually have high chemical catalytic activities owing to their large specific surface area. The chemical catalytic property of Ag/RGO was investigated with respect to the reduction of MB by $NaBH_4$ in an aqueous solution, where the concentration of $NaBH_4$ was much higher than that of MB (~20 times high); therefore, the reduction of MB can be considered as a pseudo-first-order reaction in kinetics [25]. Without adding Ag/RGO, the blue mixture showed no changes in color after three days [26]; however, if a small amount of Ag/RGO was added, the color started to fade gradually and vanished eventually within ~2 h. The catalytic progression could be precisely monitored by UV-*vis* spectroscopy. As shown in Fig. 4a, the λ_{max} absorbance at 661 nm (characteristic peak of MB) decreases over the course of the reaction, and the relationship of the change in the absorbance *versus* time fits well with the first-order kinetics as described by the equation (1) [27]:

$$\ln\left(\frac{A_t - A_\infty}{A_0 - A_\infty}\right) = -kt \qquad (1)$$

where t is the reaction time after adding Ag/RGO, A_0 is the initial absorbance, A_t and A_∞ are the absorbance at time t and when the reaction is terminated, respectively. k is the observed rate constant. In this reaction, the k of the Ag/RGO catalyst is calculated to be 2.3×10^{-4} s^{-1} (0.014 min^{-1}). Table 1 shows the catalytic rate constant of MB reduction by $NaBH_4$ with noble metals. The observed rate constant for Ag/RGO seems to be lower than those for noble metal-based catalysts reported. However, the actual amount of Ag NPs in Ag/RGO is about 7.0 wt%, and the corresponding concentration of Ag catalyst (~2.9×10^{-5} M) is extremely low compared to pure catalysts [28, 29]. It clearly indicates that the Ag/RGO composite still possesses a considerable catalytic activity. The low dosage of Ag can reduce the contamination of heavy metals and the cost as well. Furthermore, the particle size (5.6 nm) of Ag NPs in Ag/RGO is much smaller than those of metal NPs reported, and this enables a large accessible surface and an essential contribution to high catalytic activity.

The catalysis mechanism could be explained as follows [30, 31]. Generally, BH_4^- is nucleophilic relative to Ag NPs while MB is electrophilic. In the catalytic reaction, the former could

transport electrons to Ag NPs and the latter would capture electrons from Ag NPs, *i.e.*, Ag NPs serve as an electron transmitter in the system. In addition, the electronic interaction between Ag NPs and RGO is also strongly related to high catalytic activity of Ag/RGO, as the conjugate plane structure of graphene can store and release electrons like an "electron-pool" [32]. Furthermore, Ag NPs anchored onto graphene could prevent them from aggregating, thereby ensuring that the catalytic reactions proceed favorably on the surface of Ag NPs, and such graphene-metal nanocomposites could be easily recycled from the reaction system and reused for continuous catalysis applications compared to those single-component MNPs.

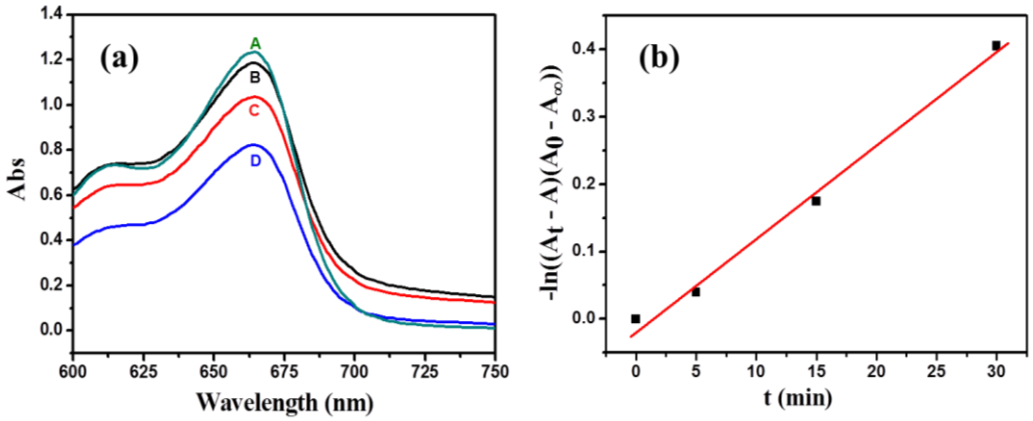

Figure 4. (a) UV-vis spectra of MB by catalytic reduction in the presence of Ag/RGO after 3 min (B), 15 min (C), and 30 min (D); (b) the first-order analysis according to equation (1).

Table 1. Rate of MB reduction by $NaBH_4$ with various Ag- and Au-based catalyst.

Catalyst materials	Particle size (nm)	First order rate constant (min^{-1})	Reference
Ag NPs	32	0.49	[29]
Ag NPs	8~20	0.22	[33]
	20~35	0.15	
Au NPs	12	0.24	[34]
Ag nanowires	65 nm in diameter	0.05 ~ 0.41	[35]
Ag NPs	20	0.44	[28]
Ag/RGO	5.6	0.014	This work

3.3. Electrocatalytic Characteristics of Ag/RGO

In order to evaluate the electrocatalytic characteristics of the Ag/RGO composite, we first investigated the volt-ampere characteristics of hydrazine at both bare and Ag/RGO-modified GCE. Fig. 5a shows no obvious peaks of redox in the potential range of -200–800 mV, indicating that the electrochemical behavior of hydrazine at bare GCE is poor. However, a typical peak of 551 mV is

observed for the Ag/RGO-modified GCE, indicating that the as-prepared composite Ag/RGO greatly improved the electrooxidation of hydrazine [36].

Fig. 5b displays the CV curves of the Ag/RGO-modified electrode at various scan rates (v), where the peak currents (I_p) increase with increasing scan rate. According to the classical Randles–Sevick equation at 25°C, the relationship between I_p and v may be expressed by the following equation: $I_p = 3.01\times10^5 n[(1-\alpha)n_\alpha]^{1/2}ACD^{1/2}v^{1/2}$ [37-39], where n stand for total electron transfer numbers in the redox reaction, α is the electron transfer coefficient, n_α is the electron number in the rate determining step, A is apparent surface area (cm^2/g) of the electrode, C is the reactant concentration in the bulk solution, and D (cm^2/s) is the diffusion coefficient, respectively. When plotting I_p *versus* square root of the scan rate ($v^{1/2}$), a linear relationship was obtained in the range of 30~110 mV/s (Fig. 5c) [40]. This behavior suggests that electrochemical oxidation of hydrazine is controlled by a diffusion process [41-43]. The liner regression equation is expressed as I_p (μA) = $5.27 + 4.64\ v^{1/2}$ ($mV^{1/2}\ s^{-1/2}$), R^2 = 0.999, comparable to many previous results [37-39, 44]. Furthermore, the peak potential (E_p) also shifted positively with increasing the scan rate (Fig. 5d). There is a linear relationship between E_p and the logarithm of scan rate (log$v$), E_p = 207.9 log$v$ + 125.2 ($mV\ s^{-1}$). This reveals an irreversible electrochemical process.

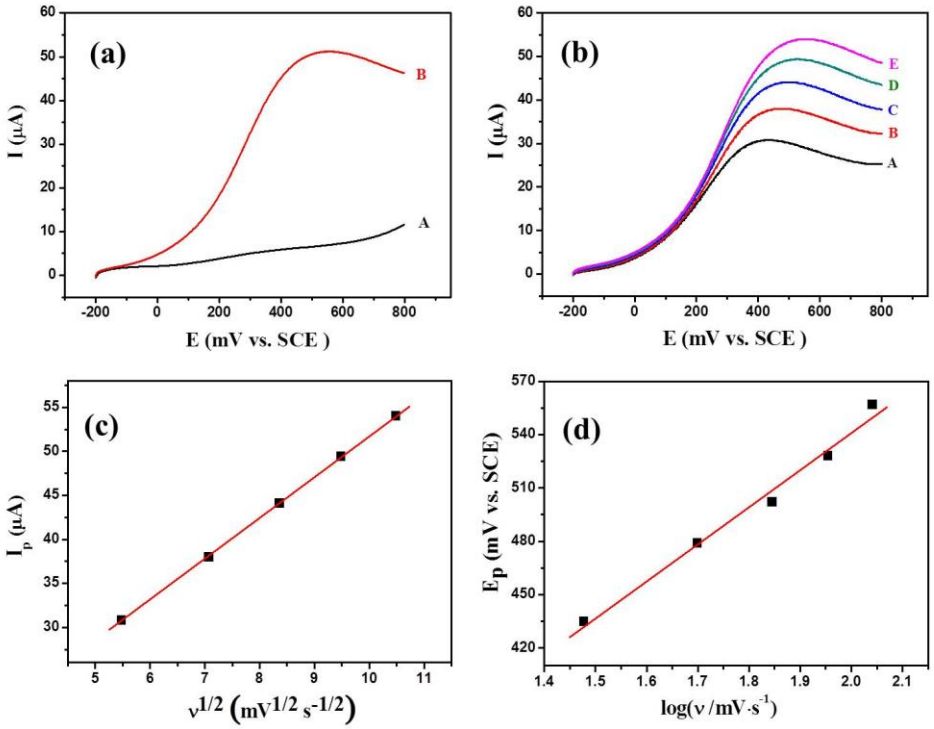

Figure 5. (a) CV curves of 10 mM hydrazine in 0.1 M K_2SO_4 solution at a scan rate of 100 mV s^{-1} with different electrodes: (A) bare GC electrode, and (B) Ag/RGO-modified GC electrodes; (b) CV curves of the Ag/RGO-modified GC electrode with various scan rates: (A) 30, (B) 50, (C) 70, (D) 90, and (E) 110 mV s^{-1}; (c) plots of I_p *vs* $v^{1/2}$; and (d) plots of E_p *vs* log$v$.

The overall oxidation reaction of hydrazine on Ag/RGO occurs via the following reaction: $NH_2NH_3^+ \rightarrow N_2 + 5H^+ + 4e$, and the generation of stable N_2 gas explains why the overall reaction is

irreversible [45, 46]. The above results indicate that the Ag/RGO composites exhibit a high electrocatalytic activity toward the electrooxidation of hydrazine and may have potential applications in fuel cells.

4. CONCLUSIONS

A two-step route was developed to prepare the Ag/RGO composites in which RGO is uniformly covered by Ag NPs with an average size of 5.6 nm. The results show that the oxygenated groups are one of key factors that determine the morphology of Ag NPs on RGO. Because Ag NPs can serve as electron transmitters in the catalytic system and have strong electronic interactions with RGO, the resulting Ag/RGO composites show high chemical catalytic activity toward the reduction of MB by $NaBH_4$. Moreover, the Ag/RGO composites also exhibit high electrocatalytic activity with an improved electrooxidation toward hydrazine.

ACKNOWLEDGEMENTS
We thank the support from the National Natural Science Foundation of China (51273057), the Program for New Century Excellent Talents in University (NCET-12-0709), the Funds for Distinguished Young Scientists in Hubei (2015CFA048), and the Chutian Scholar Program of Hubei Province (China).

References

1. X. Dong, W. Huang, P. Chen, *Nanoscale Res. Lett.*, 6 (2010) 60.
2. S. Guo, D. Wen, Y. Zhai, S. Dong, E. Wang, *ACS Nano*, 4 (2010) 3959.
3. J. Zhu, T. Zhu, X. Zhou, Y. Zhang, X. W. Lou, X. Chen, H. Zhang, H. H. Hng, Q. Yan, *Nanoscale*, 3 (2011) 1084.
4. Y. Yang, C. Han, B. Jiang, J. Iocozzia, C. He, D. Shi, T. Jiang, Z. Lin, *Mater. Sci. Eng, R*, 102 (2016) 1.
5. F. Li, H. Yang, C. Shan, Q. Zhang, D. Han, A. Ivaska, L. Niu, *J. Mater. Chem.*, 19 (2009) 4022.
6. X. Feng, R. Li, C. Hu, W. Hou, *J. Electroanal. Chem.*, 657 (2011) 28.
7. S. Stankovich, D. A. Dikin, R. D. Piner, K. A. Kohlhaas, A. Kleinhammes, Y. Jia, Y. Wu, S. T. Nguyen, R. S. Ruoff, *Carbon*, 45 (2007) 1558.
8. Y. Hernandez, V. Nicolosi, M. Lotya, F. M. Blighe, Z. Sun, S. De, I. T. McGovern, B. Holland, M. Byrne, Y. K. Gun'Ko, J. J. Boland, P. Niraj, G. Duesberg, S. Krishnamurthy, R. Goodhue, J. Hutchison, V. Scardaci, A. C. Ferrari, J. N. Coleman, *Nat. Nanotechnol.*, 3 (2008) 563.
9. S. Yoon, I. In, *Chem. Lett.*, 39 (2010) 1160.
10. Y. Xu, H. Bai, G. Lu, C. Li, G. Shi, *J. Am. Chem. Soc.*, 130 (2008) 5856.
11. Y. K. Yang, C. E. He, R. G. Peng, A. Baji, X. S. Du, Y. L. Huang, X. L. Xie, Y. W. Mai, *J. Mater. Chem.*, 22 (2012) 5666.
12. J. I. Paredes, S. Villar Rodil, A. Martinez Alonso, J. M. Tascon, *Langmuir*, 24 (2008) 10560.
13. G. Goncalves, P. A. A. P. Marques, C. M. Granadeiro, H. I. S. Nogueira, M. K. Singh, J. Grácio, *Chem. Mater.*, 21 (2009) 4796.
14. C. Xu, X. Wang, *Small*, 5 (2009) 2212.
15. J. Huang, L. Zhang, B. Chen, N. Ji, F. Chen, Y. Zhang, Z. Zhang, *Nanoscale*, 2 (2010) 2733.

16. D. Luo, G. Zhang, J. Liu, X. Sun, *J. Phys. Chem. C*, 115 (2011) 11327.
17. Y. Yang, W. Zhan, R. Peng, C. He, X. Pang, D. Shi, T. Jiang, Z. Lin, *Adv. Mater.*, 27 (2015) 6376.
18. S. Pei, H.-M. Cheng, *Carbon*, 50 (2012) 3210.
19. R. Pasricha, S. Gupta, A. K. Srivastava, *Small*, 5 (2009) 2253.
20. Y. K. Yang, C. E. He, W. J. He, L. J. Yu, R. G. Peng, X. L. Xie, X. B. Wang, Y. W. Mai, *J. Nanopart. Res.*, 13 (2011) 5571.
21. W. Gao, L. B. Alemany, L. Ci, P. M. Ajayan, *Nat. Chem.*, 1 (2009) 403.
22. M. C. Hsiao, S. H. Liao, M. Y. Yen, P. I. Liu, N. W. Pu, C. A. Wang, C. C. Ma, *ACS Appl. Mater. Interfaces*, 2 (2010) 3092.
23. C. Xu, X. Wang, J. Zhu, *J. Phys. Chem. C*, 112 (2008) 19841.
24. Y. Si, E. T. Samulski, *Chem. Mater.*, 20 (2008) 6792.
25. K. B. Ayaz Ahmed, S. Subramanian, A. Sivasubramanian, G. Veerappan, A. Veerappan, *Spectrochim. Acta, Part A*, 130 (2014) 54.
26. X. Cheng, S. C. Tjong, Q. Zhao, R. K. Y. Li, *J. Polym. Sci., Part A: Polym. Chem.*, 47 (2009) 4547.
27. H. He, C. Gao, *Sci. China Chem.*, 54 (2011) 397.
28. V. K. Vidhu, D. Philip, *Spectrochim. Acta, Part A*, 117 (2014) 102.
29. V. K. Vidhu, D. Philip, *Micron*, 56 (2014) 54.
30. Z. J. Jiang, C. Y. Liu, L. W. Sun, *J. Phys. Chem. B*, 109 (2005) 1730.
31. N. R. Jana, T. Pal, *Langmuir*, 15 (1999) 3458.
32. X. Geng, L. Niu, Z. Xing, R. Song, G. Liu, M. Sun, G. Cheng, H. Zhong, Z. Liu, Z. Zhang, L. Sun, H. Xu, L. Lu, L. Liu, *Adv. Mater.*, 22 (2010) 638.
33. V. S. Suvith, D. Philip, *Spectrochim. Acta, Part A*, 118 (2014) 526.
34. B. R. Ganapuram, M. Alle, R. Dadigala, A. Dasari, V. Maragoni, V. Guttena, *Int. Nano Lett.*, 5 (2015) 215.
35. H. K. Lee, W. S. Chew, I. Y. Phang, T. Liu, X. Y. Ling, *Chem. Commun.*, 50 (2014) 5923.
36. G. W. Yang, G. Y. Gao, C. Wang, C. L. Xu, H. L. Li, *Carbon*, 46 (2008) 747.
37. M. M. Ardakani, P. E. karami, P. Rahimi, H. R. Zare, H. Naeimi, *Electrochim. Acta*, 52 (2007) 6118.
38. G. Bharath, A. Naldoni, K. H. Ramsait, A. Abdel-Wahab, R. Madhu, E. Alsharaeh, N. Ponpandian, *J. Mater. Chem. A*, 4 (2016) 6385.
39. S. P. Kim, S. G. Lee, M. Y. Choi, H. C. Choi, *J. Nanomater.*, 2015 (2015) 1.
40. M. S. Wu, P. C. J. Chiang, *Electrochem. Commun.*, 8 (2006) 383.
41. S. Guo, J. Li, W. Ren, D. Wen, S. Dong, E. Wang, *Chem. Mater.*, 21 (2009) 2247.
42. M. Ho Yang, B. G. Choi, H. Park, T. J. Park, W. H. Hong, S. Y. Lee, *Electroanalysis*, 23 (2011) 850.
43. W. Hong, H. Bai, Y. Xu, Z. Yao, Z. Gu, G. Shi, *J. Phys. Chem. C*, 114 (2010) 1822.
44. A. Benvidi, S. Jahanbani, B.-F. Mirjalili, R. Zare, *Chin. J. Catal.*, 37 (2016) 549.
45. S. Shahrokhian, M. Ghalkhani, M. Adeli, M. K. Amini, *Biosens. Bioelectron.*, 24 (2009) 3235.
46. D. J. Guo, H. L. Li, *J. Colloid Interface Sci.*, 286 (2005) 274.